Effect of electrode shape on grounding resistances — Part 1: The focus-one protocol

Ingeman-Nielsen, Thomas; Tomaškovičová, Soňa; Dahlin, Torleif

Published in:
Geophysics

DOI:
10.1190/geo2015-0484.1

2016

GEOPHYSICS, VOL. 81, NO. 1 (JANUARY-FEBRUARY 2016); P. WA159–WA167, 5 FIGS., 1 TABLE.
10.1190/GEO2015-0484.1

Effect of electrode shape on grounding resistances — Part 1: The focus-one protocol

Thomas Ingeman-Nielsen[1], Soňa Tomaškovičová[1], and Torleif Dahlin[2]

ABSTRACT

Electrode grounding resistance is a major factor affecting measurement quality in electric resistivity tomography (ERT) measurements for cryospheric applications. Still, little information is available on grounding resistances in the geophysical literature, mainly because it is difficult to measure. The focus-one protocol is a new method for estimating single electrode grounding resistances by measuring the resistance between a single electrode in an ERT array and all the remaining electrodes connected in parallel. For large arrays, the measured resistance is dominated by the grounding resistance of the electrode under test, the focus electrode. We have developed an equivalent circuit model formulation for the resistance measured when applying the focus-one protocol. Our model depends on the individual grounding resistances of the electrodes of the array, the mutual resistances between electrodes, and the instrument input impedance. Using analytical formulations for the potentials around prolate and oblate spheroidal electrode models (as approximations for rod and plate electrodes), we have investigated the performance and accuracy of the focus-one protocol in estimating single-electrode grounding resistances. We also found that the focus-one protocol provided accurate estimations of electrode grounding resistances to within $\pm 7\%$ for arrays of 30 electrodes or more when the ratio of instrument input impedance to the half-space resistivity was 1000 m^{-1} or more. The focus-one protocol was of high practical value in field operations because it helped to optimize array installation, electrode design, and placement. The measured grounding resistances may also be included in future inversion schemes to improve data interpretation under difficult environmental conditions such as those encountered in cryospheric applications.

INTRODUCTION

Electrode grounding resistance is a major factor affecting the measurement quality in electric resistivity tomography (ERT) measurements. This was recognized in the early development and application of the resistivity method by, e.g., Rooney and Gish (1927), who report on high grounding resistances limiting the current injection and the sensitivity of their potential galvanometer. Such issues have continued to challenge generations of geophysicists because the limitations on total transmitted current lead to lower measured potentials and lower signal-to-noise levels (Dahlin and Loke, 1998; Dabas et al., 2000; Ishikawa, 2008; Doetsch et al., 2015). In severe cases, especially when ground freezing or drying is involved, grounding resistances may be so high that the transmitter circuitry loses the ability to properly regulate the current (or transmit at all) so that valid measurements cannot be obtained (Hilbich et al., 2009; Doetsch et al., 2015; Tomaškovičová et al., 2016).

Several techniques to reduce the grounding resistance problem have been reported. Enlarging the surface area of the electrodes in contact with the soil is a common strategy. It may be achieved by inserting the rod electrodes in the ground as deep as possible (Telford et al., 1990; Zonge et al., 2005), or using other electrode geometries, such as wire meshes (Zonge et al., 2005) or plates (Doetsch et al., 2015). Multiple electrodes may also be inserted in parallel (Reynolds, 1997; Kneisel and Hauck, 2008; Zonge et al., 2005). Electrodes may be watered with fresh or saline water (Telford et al., 1990; Reynolds, 1997; Zonge et al., 2005, Rosset et al., 2013) or conductive gels may be applied (Athanasiou et al., 2007), and detergents may be added to decrease water surface tension,

Manuscript received by the Editor 11 September 2015; revised manuscript received 7 October 2015; published online 29 January 2016.
[1]Technical University of Denmark, Department of Civil Engineering, Arctic Technology Centre, Lyngby, Denmark. E-mail: tin@byg.dtu.dk; soto@byg.dtu.dk.
[2]Lund University, Engineering Geology, Lund, Sweden. E-mail: torleif.dahlin@tg.lth.se.

thereby facilitating the wetting of electrode and grain surfaces (Zonge et al., 2005). Installing electrodes in clay or mud mixed with water helps to retain moisture over the course of measurements (Reynolds, 1997; Zonge et al., 2005). Measurements on rock may be performed by placing water-soaked sponges between the rock and the electrode (Kneisel and Hauck, 2008) or using expansion bolts as electrodes in holes drilled into the rock surface (Van Schoor and Binley, 2010).

Such recommendations typically originate from practical field experiences by practitioners working hard to alleviate the grounding-resistance-related problems, based on the theoretical understanding that electrode size and interfacial resistance are important factors.

In spite of the obvious significance of the problem, very little information is available in the geophysical literature about the grounding resistance of different electrode types and shapes. Calculation of the theoretical electrode grounding resistance is possible for simple electrode shapes through analytical formulations (Sunde, 1949; Wait, 1982; Ingeman-Nielsen and Tomaškovičová, personal communication, 2015) and for more complex electrode geometries by numerical modeling (Rücker and Günther, 2011).

Sunde (1949) describes a method to derive the single electrode grounding resistance based on the pairwise differential resistance measurements of three electrodes, provided that the electrodes are so distantly spaced that mutual resistance effects between the electrodes may be neglected. Using this approach, Hessler and Franzke (1958) measure the grounding resistances of large electrodes in a permafrost-affected area, and they observe up to three orders of magnitude difference in grounding resistance between the summer (thawed) and winter (frozen) season.

However for electrode layouts with short electrode spacings, such as those typically used in near-surface investigations for environmental or geotechnical projects, this method is not applicable. In practical field applications, electrode grounding is typically tested using a pairwise electrode contact test, which indicates whether current can be transmitted using a specific pair of electrodes. It also provides a circuit resistance that is indicative of the grounding resistances of the two electrodes involved, but, in general, the true single electrode grounding resistance cannot be measured.

In this paper, we present the focus-one measurement protocol, which may be used in field experiments to provide an estimate of the single-electrode grounding resistance for individual electrodes in multielectrode arrays used for ERT measurements. We derive the mathematical formulation of an equivalent electric circuit model of the focus-one measurement and use it to model the theoretical focus-one grounding resistances of synthetic multielectrode arrays with finite electrodes of different shapes. The purpose of the modeling is to evaluate the error of the grounding resistance measured using the focus-one protocol relative to the true single electrode grounding resistance, and thus, evaluate the applicability of the protocol to estimate grounding resistances of electrodes in a field setting.

The paper is the first part of a study concerned with the impact of grounding resistances on reliability of field ERT measurements. It provides the theoretical basis for the practical experiments reported in Tomaškovičová et al. (2016), in which we compare grounding resistance measurements of different electrode designs under varying environmental conditions.

DEFINITION OF GROUNDING AND MUTUAL RESISTANCE

The grounding resistance of an electrode $R_g(\Omega)$ is the potential at the electrode surface $U(\mathrm{V})$ divided by the current injected by that electrode $I(\mathrm{A})$ (Sunde, 1949; Wait, 1982; Hördt et al. 2013) as follows:

$$R_g = \frac{U}{I}. \tag{1}$$

When multiple electrodes are in use and transmitting current, the surface potential of a particular electrode is the combined potential field at that electrode caused by current injection at each electrode. In typical four-electrode resistivity measurements, two current electrodes are used, but in fact, current may flow into or out of the ground also through the potential electrodes, due to leakage currents through the instrument receiver circuitry. Thus, in the general case of N current-carrying electrodes (where $N \geq 1$), the grounding resistance of electrode i is (Sunde, 1949) as follows:

$$R_i = \frac{\sum_{n=1}^{N} U_{i,n}}{I_i} = \frac{\sum_{n=1}^{N} I_n R_{i,n}}{I_i}, \tag{2}$$

where $R_i(\Omega)$ is the grounding resistance of electrode i, $I_i(\mathrm{A})$ is the current injected by electrode i, and $U_{i,n}(\mathrm{V})$ is the potential observed at electrode i, due to the current injected at electrode n. The value

$$R_{i,j} = \frac{U_{i,j}}{I_j}, \quad i \neq j, \tag{3}$$

is called the mutual resistance at electrode i with respect to electrode j (Sunde, 1949) and represents the potential at electrode i due to the current injected at electrode j. When $i = j$, the value is simply the grounding resistance of electrode i in the absence of any other current-carrying electrode, and it is referred to as the single-electrode grounding resistance.

COMMON MODELS OF ELECTRODE GROUNDING RESISTANCE

In standard treatment of geoelectric data, electrodes are typically considered perfectly grounded infinitesimal points. However, available in the literature are analytical solutions for the potentials around a family of spheroidal electrodes: spherical (Sunde, 1949; Wait, 1982; Lile et al., 1997; Hördt et al. 2013), prolate (Wait, 1973, 1982; Igel, 2007; Rücker and Günther, 2011), and oblate spheroidal electrodes (Ingeman-Nielsen and Tomaškovičová, personal communication, 2015). The prolate and oblate spheroidal models are ellipsoids with rotational symmetry around the major and minor axes, respectively, resulting in near-rod-shaped electrodes (prolate) and pill-shaped electrodes (oblate) (see Figure 1).

The potentials around any of the spheroidal type electrodes can be summarized in the following equation (Ingeman-Nielsen and Tomaškovičová, personal communication, 2015):

$$U(x,y,z) = \frac{\rho I}{k\pi r'},$$
$$k = \begin{cases} 2 & \text{for a homogeneous half-space} \\ 4 & \text{for a homogeneous full-space} \end{cases}, \tag{4}$$

where $\rho(\Omega\text{m})$ is the resistivity of the embedding medium and $r'(\text{m})$ is the equivalent distance. The equivalent distance is the distance from an imaginary point electrode at which the potential would be the same as at the observation point. Like theoretical point electrodes, spherical electrodes give rise to spherical isopotential surfaces. Thus, for a spherical electrode, the equivalent distance is just the distance from the center of the spherical electrode to the point of observation ($r' = r$). Prolate and oblate spheroidal electrodes give rise to prolate and oblate spheroidal isopotential surfaces (which become increasingly spherical with increasing distance from the electrode), and the equivalent distances r' for such electrodes are summarized in Table 1 according to the information from Wait (1982) and Ingeman-Nielsen and Tomaškovičová (personal communication, 2015).

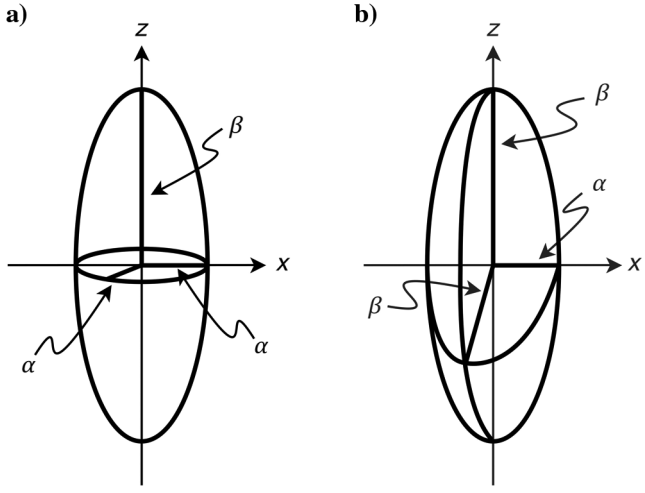

Figure 1. Illustration of the geometry of (a) prolate and (b) oblate spheroidal electrode models. They are spheroids (two axes of equal length) with rotational symmetry about the minor α and major β axis, respectively.

The surface potential of the electrode may be found by specifying the minor or major axis length of the spheroid as the x or z coordinate, taking into account the appropriate axis of rotational symmetry. For example, the spheroidal coordinate describing the surface of a prolate spheroidal electrode with rotational symmetry around the z-axis is $\eta_e = \beta/f$, where f is the semifocal distance ($f = \sqrt{\beta^2 - \alpha^2}$), β is the major axis length, and α is the minor axis length of the spheroid describing the electrode surface. Potentials for electrodes oriented with rotational symmetry around a different axis than that specified in Table 1 may be obtained by simple Cartesian coordinate transformation.

Following the derivations of Wait (1982) and Ingeman-Nielsen and Tomaškovičová (personal communication, 2015), the electrode grounding resistance of a spheroidal electrode may thus be described by the following equation:

$$R_g = R_m + R_a, \qquad R_m = \frac{\rho}{k\pi r'_e} \tag{5}$$

where r'_e is the equivalent distance from the electrode center to the surface of the electrode, also referred to as the equivalent radius of the electrode. The first term thus describes the effect of the geometry of the electrode and properties of the embedding medium $R_m(\Omega)$. The second term $R_a(\Omega)$ is an additional resistance, which may comprise an interfacial resistance component between electrode and soil, and a near-zone anomalous resistivity contribution. The value R_a may be a positive or negative term, depending on the resistivity of the anomalous zone (higher or lower than that of the embedding medium), and it may represent the change in grounding resistance from, e.g., watering of the electrode or preferential freezing or drying around the electrode. If R_a is zero, we consider the electrode to be perfectly grounded.

Mutual resistances $R_{i,j}(i \neq j)$ between spheroidal electrodes embedded in a full space may be calculated using the potential of equation 4. In this case, $r' = r'_{i,j}$ is the equivalent distance between the centers of the two electrodes $r'_{i,j}$ (Sunde, 1949), when the anomalous zones around the electrodes are small compared with the distance between them as follows:

$$R_{i,j} = \frac{U_{i,j}}{I_j} = \frac{\rho}{k\pi r'_{i,j}} \tag{6}$$

Table 1. Equivalent radius for prolate and oblate spheroidal electrodes; f is the semi focal distance $f = \sqrt{\beta^2 - \alpha^2}$, where β is the length of the major axis and α is the length of the minor axis of the electrode; i is the imaginary unit.

	Prolate spheroidal electrode	Oblate spheroidal electrode
Rotational symmetry	z-axis	x-axis
Equivalent radius	$r' = \frac{f}{Q_0(\eta)} = \frac{2f}{\ln(\frac{\eta+1}{\eta-1})}$	$r' = \frac{f}{iQ_0(i\zeta)} = \frac{2f}{i\ln(\frac{i\zeta+1}{i\zeta-1})}$
Spheroidal parameter ($y = 0$)	$\eta = \frac{\sqrt{x^2+(z+f)^2}+\sqrt{x^2+(z-f)^2}}{2f}$	$\zeta = \sqrt{\frac{\left(\sqrt{x^2+(z-f)^2}+\sqrt{x^2+(z+f)^2}\right)^2}{4f^2} - 1}$
Spheroidal parameter ($x = 0$, $y = 0$)	$\eta = \frac{z}{f}$	$\zeta = \sqrt{\frac{z}{2f^2} - 1}$
Spheroidal parameter ($z = 0$, $y = 0$)	$\eta = \sqrt{1 + \frac{x^2}{f^2}}$	$\zeta = \frac{x}{f}$

With this expression, the shape and size of the transmitting electrode j are taken into consideration, whereas the receiving electrode i is considered as an infinitesimal point. This approximation is acceptable when the distance between electrodes is large compared with their size (Ingeman-Nielsen and Tomaškovičová, personal communication, 2015).

THE FOCUS-ONE MEASUREMENT

Measuring the true single-electrode grounding resistance is not possible in practice, and only differential measurements can be performed. However, the focus-one electrode test protocol is a recent development available in commercial instruments from ABEM Instruments AB (P. Hedblom, personal communication, 2015), in which each electrode in an array is tested against all the remaining electrodes in parallel. The focus-one measurement is effectively a two-electrode measurement — current is transmitted across the same electrodes because they are used to measure the potential difference. However, the grounding resistance of half of the circuit is significantly reduced by connecting all electrodes in the array in parallel, except for the electrode under test (the focus electrode). This way, the measurement is dominated by the grounding resistance of the focus electrode. The setup is sketched in Figure 2 for an array of N electrodes with electrode n as the focus electrode. Obviously, for $N = 2$, this setup reduces to a pairwise electrode test. We present here a mathematical formulation of the circuit model of the focus-one measurement for the purpose of evaluating the focus-one resistance responses. This allows us to assert the difference between the measured focus-one resistance and the true single-electrode grounding resistance through forward modeling, while taking into account any leakage current caused by the finite internal resistance of the instrument (the input impedance).

We set up a system of linear equations to find the individual electrode currents and relevant potentials measured by the instrument. We find that, for each electrode:

$$U_i = \sum_{j=1}^{N} I_j R_{i,j} \Leftrightarrow \left(\sum_{j=1}^{N} I_j R_{i,j}\right) - U_i = 0. \tag{7}$$

For the currents passing through the electrodes and instrument internal resistance, we may write as follows:

$$I_1 + \cdots + I_{n-1} + I_{n+1} + \cdots + I_N = -I_n, \tag{8}$$

$$I = -I_n + I_v, \tag{9}$$

where $I_v(\mathrm{A})$ is the leakage current through internal resistance $R_v(\Omega)$ of the instrument. Finally, for the measured potentials:

$$I_v R_v - U_A + U_B = 0, \tag{10}$$

where $U_B(\mathrm{V})$ is the potential at the focus electrode n and U_A is the potential of the remaining $N-1$ electrodes, assuming perfectly conducting wires connect the electrodes and instrument.

Equations 7–10 can be expressed in matrix notation as follows:

$$\begin{bmatrix}
R_{1,1} & \cdots & R_{1,n-1} & R_{1,n} & R_{1,n+1} & \cdots & R_{1,N} & 0 & -1 & 0 \\
\vdots & & \vdots & \vdots & \vdots & & \vdots & \vdots & \vdots & \vdots \\
R_{n-1,1} & \cdots & R_{n-1,n-1} & R_{n-1,n} & R_{n-1,n+1} & \cdots & R_{n-1,N} & 0 & -1 & 0 \\
R_{n,1} & \cdots & R_{n,n-1} & R_{n,n} & R_{n,n+1} & \cdots & R_{n,N} & 0 & 0 & -1 \\
R_{n+1,1} & \cdots & R_{n+1,n-1} & R_{n+1,n} & R_{n+1,n+1} & \cdots & R_{n+1,N} & 0 & -1 & 0 \\
\vdots & & \vdots & \vdots & \vdots & & \vdots & \vdots & \vdots & \vdots \\
R_{N,1} & \cdots & R_{N,n-1} & R_{N,n} & R_{N,n+1} & \cdots & R_{N,N} & 0 & -1 & 0 \\
0 & \cdots & 0 & 0 & 0 & \cdots & 0 & R_v & -1 & 1 \\
1 & \cdots & 1 & 1 & 1 & \cdots & 1 & 0 & 0 & 0 \\
1 & \cdots & 1 & 0 & 1 & \cdots & 1 & 1 & 0 & 0
\end{bmatrix}
\cdot
\begin{bmatrix}
I_1 \\ \vdots \\ I_{n-1} \\ I_n \\ I_{n+1} \\ \vdots \\ I_N \\ I_v \\ U_A \\ U_B
\end{bmatrix}
=
\begin{bmatrix}
0 \\ \vdots \\ 0 \\ 0 \\ 0 \\ \vdots \\ 0 \\ 0 \\ 0 \\ I
\end{bmatrix}. \tag{11}$$

Equation 11 is of the form $\underline{\underline{\mathbf{A}}}\mathbf{x} = \mathbf{b}$ and can be solved as $\mathbf{x} = \underline{\underline{\mathbf{A}}}^{-1}\mathbf{b}$. After solution, the solution vector $\mathbf{x}$ holds the currents transmitted by the individual electrodes I_i, the leakage current through the instrument I_v, and the two potentials U_A and U_B. The measured focus-one resistance may be calculated as follows:

$$R = \frac{U_A - U_B}{I}. \tag{12}$$

In the simplest case in which the layout consists of only two electrodes ($N = 2$), the measured resistance reduces to the simple representation as follows:

$$R = (R_{1,1} - R_{1,2} - R_{2,1} + R_{2,2}) \times \frac{R_v}{R_{1,1} - R_{1,2} - R_{2,1} + R_{2,2} + R_v}. \tag{13}$$

The first factor in equation 13 represents the ideal circuit resistance. The second term represents the effect of current leakage through the instrument, and it is equivalent to the system factor introduced by Ingeman-Nielsen and Tomaškovičová (personal communication, 2015). For identical electrodes in a homogeneous medium (half- or full-space), the mutual and grounding resistances are linearly dependent on the medium resistivity, and the system factor may be represented as follows:

$$F_s = \frac{R_v/\rho}{K + R_v/\rho}, \tag{14}$$

where K is a term that depends only on the electrode shape and layout geometry. From this formulation, we observe that the measured resistance scales with the ratio of instrument input impedance to medium resistivity R_v/ρ. Through numerical modeling of layouts with up to 1000 electrodes, we have confirmed this observation for the focus-one protocol in general.

Whenever electrodes are identical in shape and properties or distantly spaced, the reciprocity principle ($R_{i,j} = R_{j,i}$) may be applied in equations 11 and 13 to reduce the computational effort.

MODELING RESULTS

Focus-one resistance errors for perfectly grounded electrodes

The derivation has been used to investigate the theoretical errors in measured focus-one resistance relative to the true single-electrode grounding resistance for arrays with three different electrode geometries (see Figure 3): (1) prolate spheroidal electrodes ($\alpha = 0.5$ cm, $\beta = 10$ cm) inserted vertically (major axis) into a homogeneous half-space, (2) oblate spheroidal electrodes ($\alpha = 0.5$ mm, $\beta = 8$ cm) inserted vertically into a homogeneous half-space, with the minor axis oriented in the length direction of the electrode layout, and (3) buried horizontal prolate spheroidal

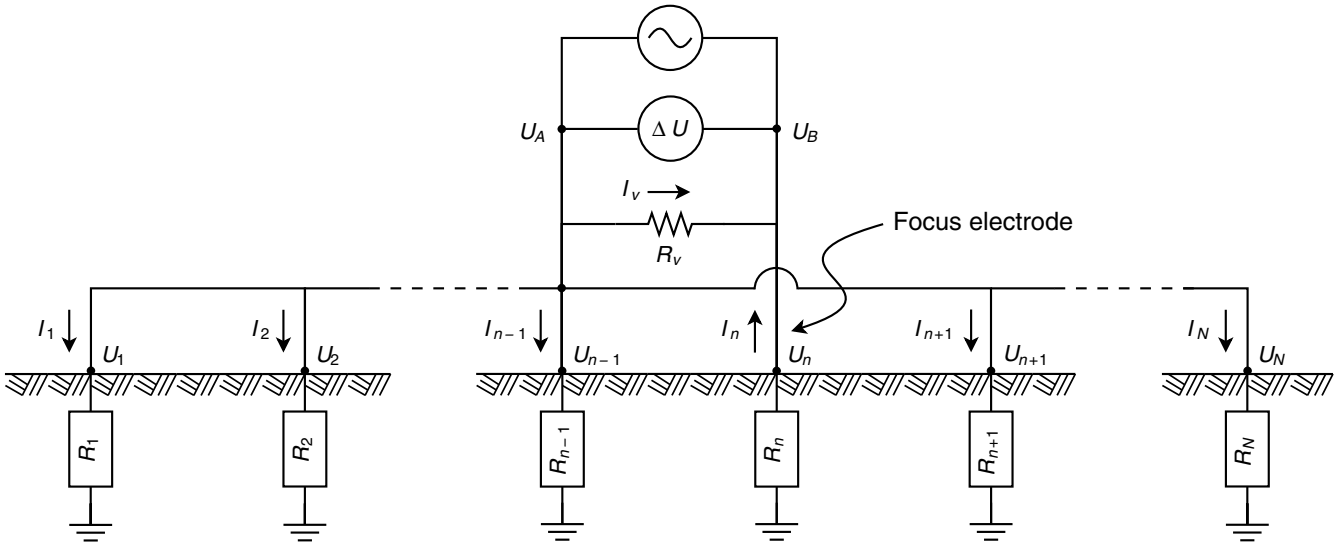

Figure 2. Equivalent circuit diagram of the focus-one measurement over an array of N electrodes with electrode n as the focus electrode. Mutual effects between electrodes are not represented.

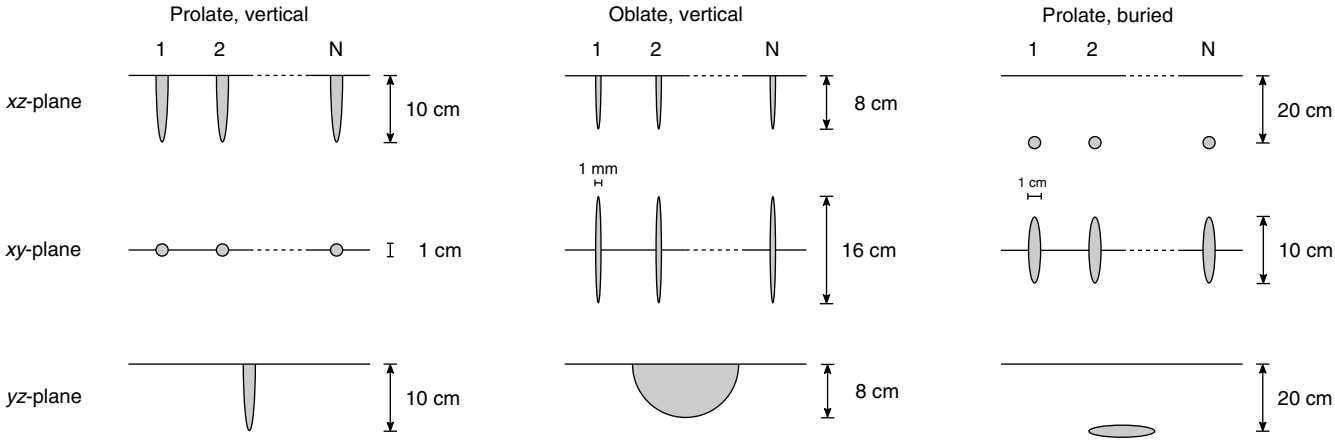

Figure 3. The electrode arrays investigated consist of N electrodes equidistantly positioned along the x-axis. Three electrode geometries are investigated: (1) vertical prolate spheroidal electrodes with the major axis in the z-direction, (2) vertical oblate spheroidal electrodes with the minor axis in the x-direction, and (3) buried prolate spheroidal electrodes with the major axis in the y-direction (perpendicular to the array direction). The figure is not to scale.

electrodes ($\alpha = 0.5$ cm, $\beta = 5$ cm) with the major axis oriented in the y-direction (perpendicular to the electrode layout) and buried at a depth of 0.2 m. In the case of buried electrodes, grounding resistances are calculated by introducing imaginary image electrodes above the ground surface (Sunde, 1949; Daniels, 1978). Modeling results are presented in Figure 4 as a function of the number of electrodes in the layout (electrode count, N) for different choices of focus electrode, electrode spacing, and R_v/ρ, whereas all electrodes are considered perfectly grounded. The calculated focus-one to single-rod resistance errors are plotted as absolute values ($|R/R_g^{N=1} - 1|$) to allow logarithmic axes.

We observe that the measured focus-one resistance is close to twice the single electrode grounding resistance when a two-electrode setup is measured, and it decreases with increasing electrode count as expected. For layouts with relatively small electrode spacing, the measured focus-one resistance actually becomes less than the single-electrode grounding resistance (the error is negative) for sufficiently large electrode counts due to the mutual resistance effects.

The error depends on the choice of focus electrode (see Figure 4a and 4b). Electrodes at the ends of the layout are less affected by mutual effects, and thus the measured focus-one resistance is less reduced for larger electrode counts. This edge effect is quickly reduced as the focus electrode is moved toward the center of the layout. This is clear from the relatively small change in error observed when comparing the center electrode with an electrode at a distance of one-tenth of the total electrode array length.

The measured error is strongly dependent on the chosen electrode separation. For large separations, the mutual effects are insignificant and the error simply decreases with the increasing electrode count. Mutual effects become increasingly important for short electrode spacings causing the sign change of the error to occur at smaller electrode counts. This effect is more pronounced for oblate than for prolate spheroidal electrodes as shown in Figure 4c and 4d.

Finally, the error depends on the ratio of instrument input impedance to half-space resistivity. For smaller ratios, the reduction in measured focus-one resistance increases, the electrode count needed to cause the sign change in the error is reduced, and the absolute value of the error at large electrode counts is increased. This effect is more pronounced for prolate than oblate spheroidal electrodes (see Figure 4e and 4f).

Although burial of the electrodes effectively reduces the theoretical single-electrode grounding resistance, the modeling showed that the change in the focus-one resistance error was minimal at less than 1% (results not shown).

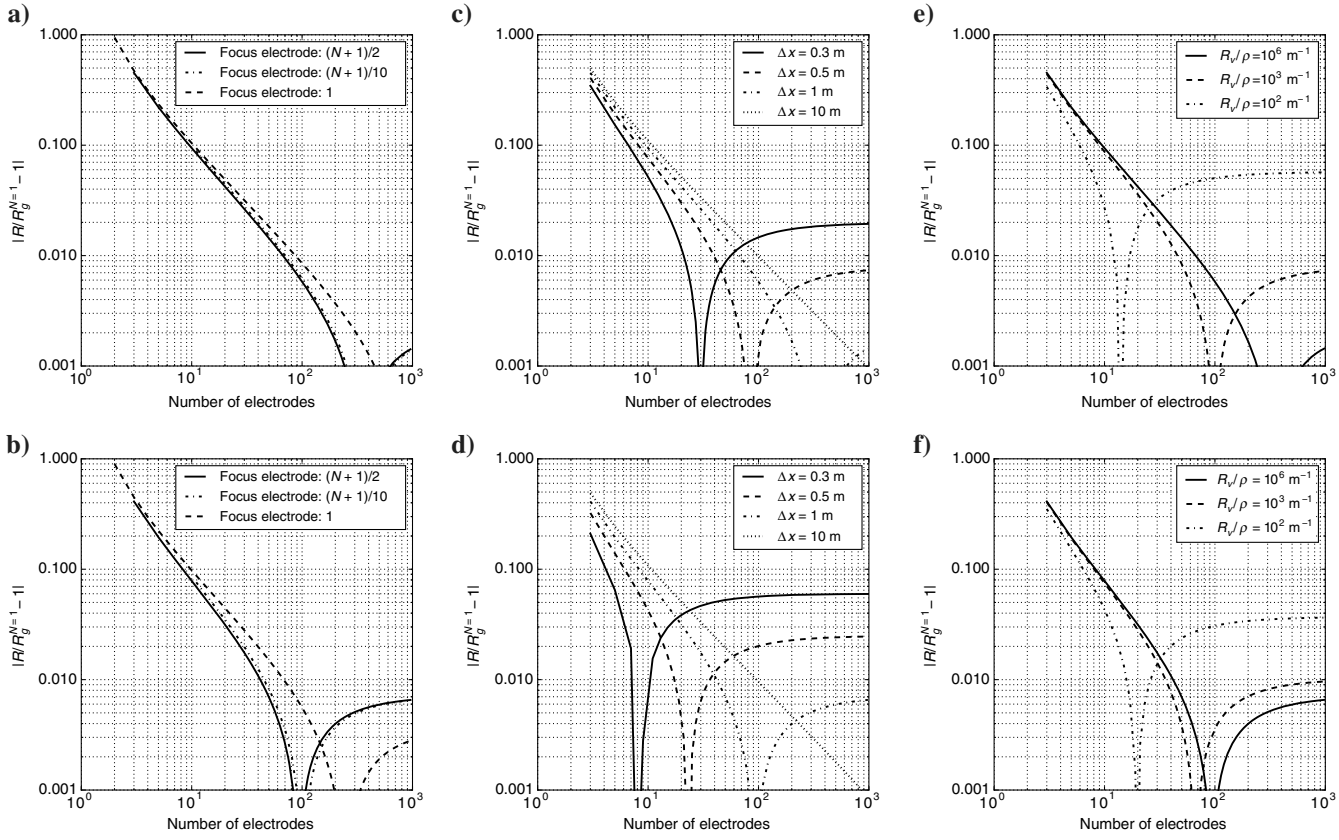

Figure 4. Absolute value of the error in measured focus-one resistance to single electrode grounding resistance for prolate ($\alpha = 0.5$ cm, $\beta = 10$ cm, plots a, c, and e) and oblate spheroidal electrodes ($\alpha = 0.5$ mm, $\beta = 8$ cm, plots b, d, and f). Plots (a and b) show errors for different choices of focus electrode using an electrode spacing of 1 m and infinite instrument input impedance. Plots (c and d) show errors for different choices of electrode spacing using a focus electrode at the center of the layout and infinite input impedance. Plots (e and f) show errors for different values of the ratio R_v/ρ, using a focus electrode at the center of the layout and an electrode spacing of 1 m. All electrodes are considered perfectly grounded. Note that the plots show the absolute value of the error, which is always positive for small electrode counts and may turn negative for large counts.

Effect of additional grounding resistance on focus-one resistance

The effect of additional grounding resistance has been studied under the assumption that the additional resistances of all electrodes in a layout are lognormally distributed with a scale e^{μ} and shape σ such that $\log_e(R_g)$ is normally distributed with mean μ and standard deviation σ.

For each choice of electrode count from 2 to 1000, we report the mean and standard deviation of 1000 repeated calculations of the focus-one resistance. These repetitions use random sampling of a specific lognormal distribution for the additional resistance of the (nonfocus) electrodes. Based on the field observations by Tomaškovičová et al. (2016), we chose three values of e^{μ} at [3, 30, and 300 kΩ] and $\sigma = 0.4$. For each distribution, we studied a focus electrode at the center of the array with additional resistance R_a equal to $e^{\mu-2\sigma}$, e^{μ}, and $e^{\mu+2\sigma}$, (see Figure 5a).

We find that when R_a is small compared with R_m (the contribution of the embedding media; see equation 5), the errors induced by the additional grounding resistance are insignificant and the total focus-one resistance error is similar to the perfectly grounded case. Because R_a is increased, the measured focus-one resistance error (mean of 1000 repeated calculations) depends mainly on the additional grounding resistance of the focus electrode. A focus electrode additional resistance of less than e^{μ} results in larger errors (fewer negative for high electrode counts), whereas a focus electrode additional resistance larger than e^{μ} results in smaller errors (more negative for high electrode counts). The variation observed due to the repeated random sampling for electrode additional resistances is larger for layouts with few electrodes and decreases with an increasing electrode count. As an example, results are shown in Figure 5b for prolate spheroidal electrodes ($\alpha = 0.5$ cm, $\beta = 10$ cm) at the surface of a homogeneous half-space of 10,000 Ωm for an instrument input impedance of 10 MΩ and an electrode spacing of 1 m.

Our complete model suite included prolate and oblate electrodes at the surface of a half-space and prolate electrodes buried at a depth of 20 cm. Electrode dimensions and geometry were the same as previously described. Electrode separations varied from 0.3 to 1 m, and the ratio R_v/ρ varied between 300 and 10^5 m^{-1}. Figure 5c shows the first and 99th percentile errors of the modeled focus-one resistances relative to the single-electrode grounding resistance for arrays with electrode counts from three to 1000 and varying values of the R_v/ρ ratio. The maximum error observed is better than ±7% across all model scenarios for arrays of 30 electrodes or more, provided R_v/ρ ratio is larger than 1000 m^{-1}. However, for longer electrode arrays (larger electrode counts), the grounding resistance is more likely to be underestimated than overestimated.

THE EFFECT OF SQUARE AND CYLINDRICAL ELECTRODES

Using prolate and oblate electrode models have allowed us to use fast and simple analytical solutions for the modeling exercises. For practical reasons in field surveys, however, the electrodes would typically be cylindrical rods or square plates rather than prolate and oblate spheroids.

To evaluate the error introduced by the spheroidal approximation, we have used COMSOL Multiphysics to produce numerical models of a square plate of similar areal extent as the oblate model in the presented modeling, and a cylindrical rod of the same length as the prolate model was used. Both were inserted vertically into a homogeneous half-space.

The square electrode modeled had dimensions of $10 \times 10 \times 0.1$ cm ($h \times w \times t$), and the surface potential was 6% lower than that of the equivalent oblate spheroidal model ($\alpha = t$ and $\beta = \sqrt{\pi \times h \times w}$), which translates directly to a 6.0% error in single electrode grounding resistance. At 0.3 m distance from the electrode surface (perpendicular to the plate surface and at the ground surface), the difference in potential was less than 0.8%.

The cylindrical rod electrode was 1 cm in diameter d, 10 cm long l, and it was conical at the lower 2 cm, which is customary for ease of installation. The surface potential was 5.7% lower than that of the equivalent prolate spheroidal model ($\alpha = d/2$ and $\beta = l$). At 0.3 m distance from the electrode surface (at the ground surface), the difference in potential was less than 0.5%.

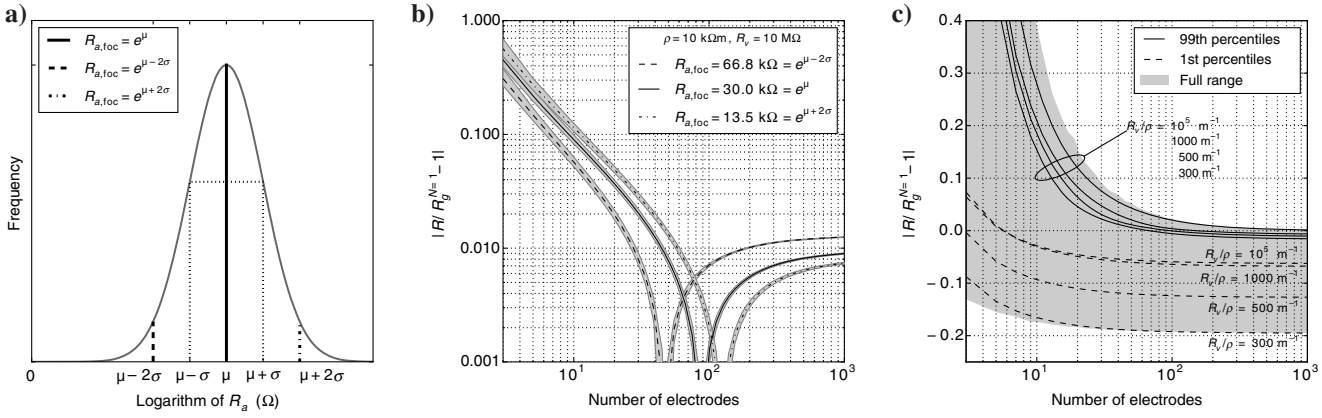

Figure 5. Examples of the error in modeled focus-one resistance relative to true single-electrode grounding resistance, when the additional grounding resistances of the layout electrodes are assumed to follow a lognormal distribution. Panel (a) shows the three choices of focus electrode additional resistance modeled for each distribution. (b) Example of model results for prolate spheroidal electrodes ($\alpha = 0.5$ cm, $\beta = 10$ cm) at the surface of a homogeneous half-space. The black lines are 50th percentiles, and the shaded areas represent the 5th to 95th percentiles of the 1000 repetitions for each array size. (c) First and 99th percentiles for different values of R_v/ρ and max and min of the full range of models, illustrating the accuracy of the focus-one measurement for arrays of different electrode counts.

The numerical model was also tested with oblate and prolate electrode models, and we found a numerical precision of ±0.3% of the analytically calculated potential. Furthermore, we calculated the responses of the square and cylindrical models for three different half-space resistivities and confirmed that the potential fields of these electrode shapes also depend linearly on the half-space resistivity.

The focus-one to true single-electrode grounding resistance ratio ($R/R_g^{N=1} - 1$) used to plot the modeling results in Figures 4 and 5 is slightly affected by the spheroidal assumptions. Considering the relatively severe case of arrays with electrode spacings of 0.3 m, a half-space resistivity of 10 kΩm, and an instrument input impedance of 1 MΩ ($R_v/\rho = 100$ m^{-1}), the ratios based on the oblate and square electrode models typically differ by less than ±0.005 or 0.5% points. For layouts with very few electrodes, the differences may amount to as much as ±1.5% points. Based on these numerical simulations, we therefore conclude that the errors introduced by the spheroidal assumptions are so small that they have no practical significance.

THE EFFECT OF FINITE RECEIVER ELECTRODES

The present modeling considers the electrode shape and size when calculating potential fields originating from current injection of an electrode. However, in the calculation of mutual resistances, the receiver electrode is considered as a point electrode. The physical size and shape of receiver electrodes and the perturbation of the potential field caused by their presence are thus neglected. Such effects are discussed by Rücker and Günther (2011) and Ingeman-Nielsen and Tomaškovičová (personal communication, 2015), who find that the approximation is valid for electrodes that are small when compared with their separation. This condition is typically met in an array of equidistant electrodes, except possibly for neighboring electrodes. Thus, for arrays of many electrodes, we expect the effects to be insignificant. The mathematical formulation presented is general and depends on the calculated grounding and mutual resistances. These could be provided by any suitable forward modeling scheme, e.g. the numerical scheme presented by Rücker and Günther (2011), which takes the mentioned electrode effects into account at the expense of greater computational effort.

CONCLUSION

In this paper, we have presented the focus-one protocol for estimating electrode grounding resistances of multielectrode arrays used for ERT measurements. In the focus-one measurement, the resistance is measured between one single electrode (the focus electrode) and all the remaining electrodes connected in parallel. In this way, the measured resistance is dominated by, and thus, provides an estimate of the grounding resistance of the focus electrode.

We have presented a general mathematical formulation of the measured circuit resistance, taking into account the instrument input impedance and mutual effects between the electrodes of the array. Based on this formulation, the performance of the focus-one protocol was investigated using prolate and oblate spheroidal models as approximations for rod and plate electrodes inserted vertically at the surface of a homogeneous half-space.

We found that the deviations of the measured focus-one resistance compared with the true single electrode grounding resistance may be positive and negative; i.e., the focus-one resistance may be larger or smaller than the true single electrode grounding resistance, depending mainly on the mutual effects between electrodes. The largest absolute deviations occur for low electrode separations, low ratio of instrument input impedance to half-space resistivity (R_v/ρ), and high-focus electrode grounding resistance. However, for $R_v/\rho \geq 1000$ m^{-1}, the focus-one measurement typically provides an accurate estimate of the true single-electrode grounding resistance to within ±7% for arrays of 30 electrodes or more.

We attribute the focus-one protocol great practical relevance as a fast method to evaluate electrode grounding resistances in field operations and a tool to optimize array installation, electrode design, and eventually the quality of the collected data. We also foresee the use of focus-one resistances in future inversion schemes that may take instrument input impedance and electrode grounding resistances into account as a tool to improve inversion quality under difficult environmental conditions, such as those encountered in cryospheric applications.

ACKNOWLEDGMENTS

The focus-one protocol discussed in this paper was invented by P. Hedblom of ABEM Instruments AB. We wish to thank him for fruitful discussions about the implementation of the protocol in their current instrumentation.

REFERENCES

Athanasiou, E. N., P. I. Tsourlos, G. N. Vargemezis, C. B. Papazachos, and G. N. Tsokas, 2007, Non-destructive DC resistivity surveying using flat-base electrodes: Near Surface Geophysics, **5**, 263–272, doi: 10.3997/1873-0604.2007008.

Dabas, M., A. Hesse, and J. Tabbagh, 2000, Experimental resistivity survey at Wroxeter archaeological site with a fast and light recording device: Archaeological Prospection, **7**, 107–118, doi: 10.1002/1099-0763(200006)7:2<107::AID-ARP138>3.3.CO;2-S.

Dahlin, T., and M. H. Loke, 1998, Resolution of 2D Wenner resistivity imaging as assessed by numerical modelling: Journal of Applied Geophysics, **38**, 237–249, doi: 10.1016/S0926-9851(97)00030-X.

Daniels, J. J., 1978, Interpretation of buried electrode resistivity data using a layered earth model: Geophysics, **43**, 988–1001, doi: 10.1190/1.1440878.

Doetsch, J., T. Ingeman-Nielsen, A. V. Christiansen, G. Fiandaca, E. Auken, and B. Elberling, 2015, Direct current (DC) resistivity and induced polarization (IP) monitoring of active layer dynamics at high temporal resolution: Cold Regions Science and Technology, **119**, 16–28, doi: 10.1016/j.coldregions.2015.07.002.

Hessler, V. P., and A. R. Franzke, 1958, Earth-potential electrodes in permafrost and tundra: Arctic, **11**, 211–217, doi: 10.14430/arctic3746.

Hilbich, C., L. Marescot, C. Hauck, M. H. Loke, and R. Mäusbacher, 2009, Applicability of electrical resistivity tomography monitoring to coarse blocky and ice-rich permafrost landforms: Permafrost and Periglacial Processes, **20**, 269–284, doi: 10.1002/ppp.v20:3.

Hördt, A., P. Weidelt, and A. Przyklenk, 2013, Contact impedance of grounded and capacitive electrodes: Geophysical Journal International, **193**, 187–196, doi: 10.1093/gji/ggs091.

Igel, J., 2007, On the small-scale variability of electrical soil properties and its influence on geophysical measurements: Ph.D. dissertation, University of Frankfurt/Main.

Ishikawa, M., 2008, ERT imaging for frozen ground detection, *in* C. Hauck, and C. Kneisel, eds., Applied geophysics in periglacial environments: Cambridge University Press, 109–117.

Kneisel, C., and C. Hauck, 2008, Electrical methods, *in* C. Hauck, and C. Kneisel, eds., Applied geophysics in periglacial environments: Cambridge University Press, 3–27.

Lile, O. B., M. Morris, and J. S. Rønning, 1997, Estimating groundwater flow velocity from changes in contact resistance during a saltwater tracer experiment: Journal of Applied Geophysics, **38**, 105–114, doi: 10.1016/S0926-9851(97)00018-9.

Reynolds, J. M., 1997, An introduction to applied and environmental geophysics: Wiley.

Rooney, W. J., and O. H. Gish, 1927, Results of earth-resistivity surveys near Watheroo, Western Australia, and at Ebro, Spain: Terrestrial Magnetism and Atmospheric Electricity, **32**, 49–63, doi: 10.1029/TE032i002p00049.

Rosset, E., C. Hilbich, S. Schneider, and C. Hauck, 2013, Automatic filtering of ERT monitoring data in mountain permafrost: Near Surface Geophysics, **11**, 423–433, doi: 10.3997/1873-0604.2013003.
Rücker, C., and T. Günther, 2011, The simulation of finite ERT electrodes using the complete electrode model: Geophysics, **76**, no. 4, F227–F238, doi: 10.1190/1.3581356.
Sunde, E. D., 1949, Earth conduction effects in transmission systems: Dover Van Nostrand Company Inc.
Telford, W. M., L. P. Geldart, and R. E. Sheriff, 1990, Applied geophysics: Syndicate of the University of Cambridge.
Tomaškovičová, S., T. Ingeman-Nielsen, A. V. Christiansen, I. Brandt, T. Dahlin, and B. Elberling, 2016, Effect of electrode shape on grounding resistances. Part 1: Experimental results and cryospheric monitoring: Geophysics, **81**, this issue, doi: 10.1190/GEO2015-0148.1.
Van Schoor, M., and A. Binley, 2010, In-mine (tunnel-to-tunnel) electrical resistance tomography in South African platinum mines: Near Surface Geophysics, **8**, 563–574, doi: 10.3997/1873-0604.2010021.
Wait, J. R., 1973, Resistance of earth electrodes: Electronics Letters, **9**, 90–91, doi: 10.1049/el:19730068.
Wait, J. R., 1982, Geo-electromagnetism: Academic Press.
Zonge, K., J. Wynn, and S. Urquhart, 2005, Resistivity, induced polarization and complex resistivity, *in* D. K. Butler, ed., Near-surface geophysics: SEG, 265–300.